대한기계학회 2000년도 추계학술대회논문집 A pp. 736~742 KSME 00F108

# Explosive mass-removal processes during high power nanosecond Nd-YAG laser ablation of silicon

## (나노초 야그 레이저 어블레이션에 의한 실리콘의 폭발적 제거 현상)

S. H. Jeong*(정성호), J. H. Yoo**, R. Greif***, R. E. Russo**

**Key words** : Laser ablation(레이저 어블레이션), explosive boiling(폭발적 보일링), induced transparency (유도투명화)

**Abstract**

Mass removed from crystalline silicon samples during high power single-pulse laser ablation was studied by measuring the resulting crater morphology with a white light interferometric microscope. The volume and depth of the craters show a strong nonlinear change as the laser irradiance increases across a threshold value, that is, approximately $2.2\times10^{10}$ W/cm$^2$. Time-resolved shadowgraph images of the ablation plume show the ejection of large particulates from the sample for laser irradiance above the threshold, with a time delay of about 300-400 nsec. The thickness of superheated liquid layer near the critical temperature was numerically estimated, considering the transformation of liquid metal into liquid dielectric near the critical state (i.e., induced transparency). The estimated thickness of the superheated layer at a delay time of 200 nsec agreed with the measured crater depths, suggesting that induced transparency promotes the formation of a deep superheated liquid layer which leads to an explosive boiling responsible for the sudden increase of crater volume and depth.

## 1. INTRODUCTION

Laser ablation has become a dominant technology for such applications as production of nanomaterials, micromachining of metalic and nonmetalic solid samples, deposition of thin films, welding and bonding of metal parts, and chemical analysis.[1-5] For these applications, an understanding of the relationship between the quantity and size of ablated mass versus the laser irradiance is crucial in selecting optimum process parameters. Laser ablation involves complex and collective mass-removal mechanisms. An identification of relevant mechanisms is the key to accurately estimating ablated mass at a given laser irradiance. Depending on the laser irradiance, the mass may be removed in the form of fine vapor, liquid droplets, or solid flakes.[2,6]

The removal of mass from the irradiated zone can occur by both thermal and nonthermal mechanisms. Incident laser radiation on metal or semiconductor samples creates a large population of highly excited nonequilibrium electrons in a region near the sample surface. This electronic excitation can lead to bond breaking of the sample material and subsequently can cause atomic-size particles to be ejected from the surface.[6] For a thermal mechanism, the excited electrons transfer energy to lattice and this energy is redistributed through lattice vibrations to heat the sample. The heating of a solid sample above the boiling temperature leads to the evaporation of the material to remove atomic-size mass. Mass removal in the form of micron-sized droplets can also result from hydrodynamic instability of the molten liquid layer.[7,8] For laser intensities exceeding about $10^9$ W/cm$^2$, heating the sample above the boiling temperature is possible and, as a result, a superheated metastable liquid layer may form. It was reported that homogeneous nucleation within this superheated liquid layer is a possible mechanism responsible for mass removal during high power laser heating.[9,10]

In this work, ablation of polished pure silicon samples during laser irradiation ($10^9$-$10^{11}$ /cm$^2$) was investigated by measuring the crater characteristics. Laser shadowgraphy was used to image the ejected mass from the surface, to approximately estimate its size, and to infer the time scale for the onset of mass ejection. Based on crater volume data, the shadowgraph images, and a numerical calculation for superheated liquid layer thickness during and after the laser pulse, it is proposed that explosive boiling (phase explosion) may be a dominant mechanism for mass removal for laser irradiances greater than $2.2\times10^{10}$ W/cm$^2$.

## 2. EXPERIMENTAL SYSTEM

A schematic diagram of the experimental system is shown in Fig.1. A frequency-quadrupled Nd-YAG laser (Coherent, Model Infinity 40-100) with wavelength and pulse duration of 266 nanometer (nm) and 3 nanosecond (nsec) at the full width half maximum, respectively, was

* Kwangju Institute of Science and Technology, Department of Mechatronics
** Lawrence Berkeley National Laboratory, U.S.A.
*** University of California at Berkeley, U.S.A.

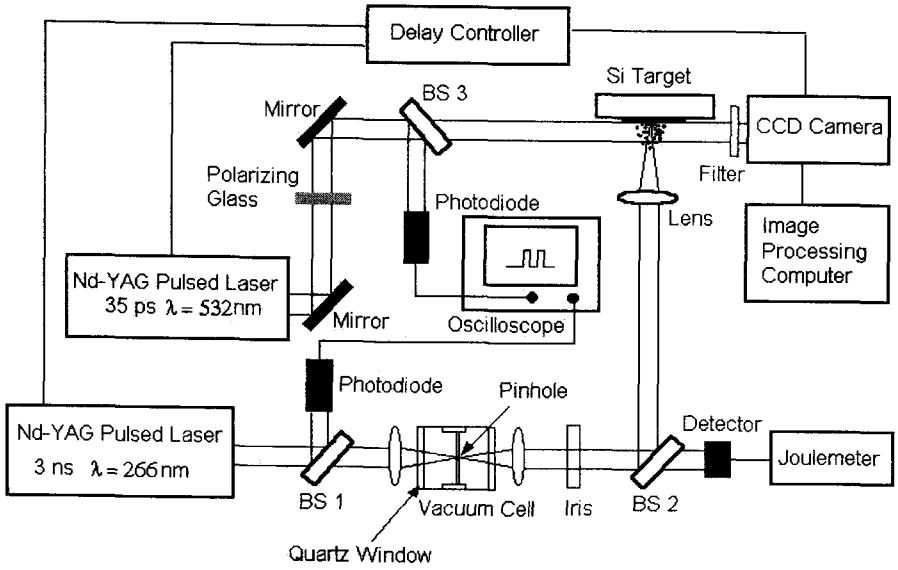


Fig.1 Schematic diagram of the experimental system

used to irradiate the target. The laser beam was shaped into a nearly Gaussian profile by passing a pinhole and focused with a plano-convex quartz lens ($f$=20 cm) to approximately 50 μm diameter on the silicon target. The laser pulse energy delivered to the target was measured with a pyroelectric detector and a calibrated joulemeter by collecting a known fraction of the laser beam with a beam splitter (BS2). A polished single crystal silicon wafer (99.99% purity) diced to 1×2 cm rectangular pieces was used as the ablation sample. The laser fluence ranged from 5 to 400 J/cm$^2$, which results in irradiance of approximately $1\times10^9$ to $1\times10^{11}$ W/cm$^2$. All experiments in this work were conducted using a single laser pulse on a fresh surface location. The morphology, depth, and volume of the craters were measured with a white light interferometric microscope (Zygo, Model NewView 200).

A picosecond Nd-YAG laser (Continuum, Model YG601) with wavelength and pulse duration of 532 nm and 35 psec, respectively, was used as a probe beam for the shadowgraph imaging of mass ejection from the silicon surface. The probe beam was aligned parallel to the silicon surface and perpendicular to the ablation beam. A polarizing glass filter was used to adjust the intensity of the probe beam, keeping the CCD camera (Photometrics, Model CH250/A) from saturation. A narrow-band filter was placed in front of the CCD camera to block the plume radiation. The time interval between the ablation pulse and the probe pulse was controlled with a digital delay/pulse generator (Stanford Research Systems, Model DG535). To measure the actual time delay between the probe and the ablation pulses, which could be different from the preset value due to electronic jitter, a portion of the beam was delivered to a fast ultraviolet (UV) photodiode using a beam splitter (BS 1 or BS 3). By measuring the time difference between the two photodiode-signals with a digital oscilloscope (Tektronix, Model DSA 602A), the time delay of the probe pulse with respect to the ablation beam was obtained. At each selected laser irradiance, time-resolved images of mass ejection above the silicon surface were acquired by varying the delay from 5 nsec to 30 μsec.

## 3. RESULTS AND DISCUSSION

### 3.1 Experiment

Figure 2 shows the measured crater volume and depth as a function of laser irradiance for a beam diameter of about 50 μm. The crater depth and volume undergo a dramatic increase at the irradiance of about $2.2\times10^{10}$ W/cm$^2$. As the irradiance is increased from $1.9\times10^9$ to $2.2\times10^{10}$ W/cm$^2$, the crater depth increases gradually from 0.4 to 1.8 μm. At $2.2\times10^{10}$ W/cm$^2$, the crater depth abruptly increases from 1.8 to 6 μm, more than a threefold increase in the ablation depth. The crater depth increases rapidly from 6 to 19 μm for increasing laser irradiance from $2.2\times10^{10}$ to $9.5\times10^{10}$ W/cm$^2$.

The crater shape at laser irradiances below and above the threshold value of $2.2\times10^{10}$ W/cm$^2$ is completely different. Figure 3 shows cross-sectional views of the craters at selected laser irradiances of $2.0\times10^{10}$ and $2.4\times10^{10}$ W/cm$^2$, which are slightly below and above the threshold irradiance. For irradiance below $2.2\times10^{10}$ W/cm$^2$, the craters exhibit a rather hemispherical shape with a rim above the surface. The rim is believed to result from the resolidification of molten silicon around the edge of the crater. The circular ripples near the edge

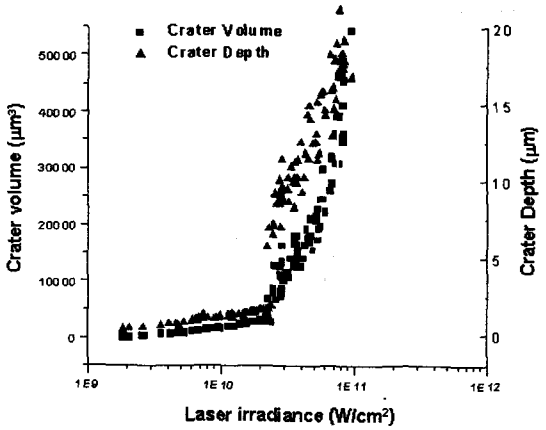


Fig.2 Crater volume and depth as a function of laser irradiance, showing an abrupt increase at $2.2\times10^{10}$ W/cm$^2$

of the crater may result from the motion of the molten silicon induced by a lateral pressure gradient between the high pressure plasma above the sample surface and the surrounding ambient. When the laser irradiance is increased above $2.2\times10^{10}$ W/cm$^2$, the crater shape changes to one with a deep hole near the center and a rim at the very edge of the crater. The bottom of the crater is now rough with several local peaks and valleys. Scanning electron microscope images of the craters for laser irradiance below and above the threshold value also showed very different morphology. For the craters above the threshold, many resolidified micron-size droplets were present near the deep hole and the surrounding surface (cf. Fig. 4).

Time-sequenced images of ejected mass at selected laser irradiances were obtained using laser shadowgraphy. These images reveal that the formation of the deep crater structure produced at about $2.2\times10^{10}$ W/cm$^2$

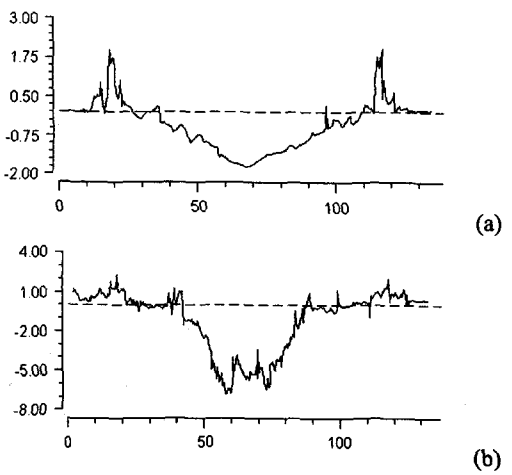


Fig.3 Cross-sectional view of the craters at slightly below and above the threshold laser irradiance, $2.2\times10^{10}$ W/cm$^2$; (a) $2.0\times10^{10}$ and (b) $2.4\times10^{10}$ W/cm$^2$

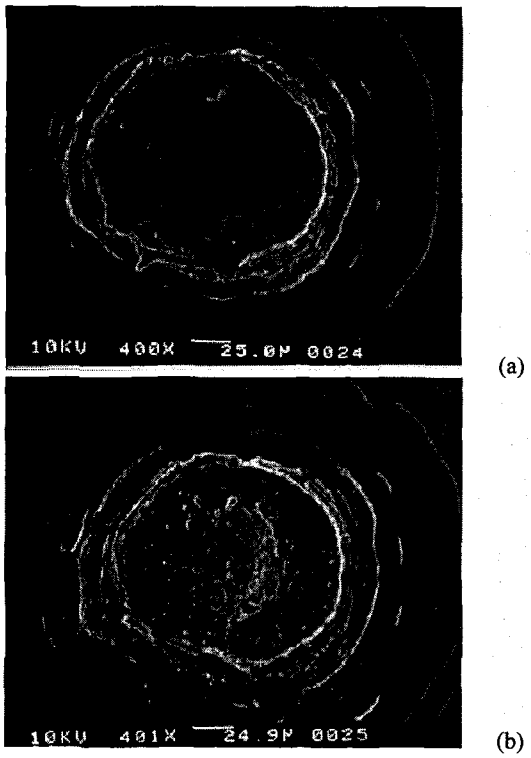


Fig.4 Scanning electron microscope images of the crater for (a) laser irradiance slightly below the threshold and (b) laser irradiance slightly above the threshold. Laser spot diameter for these images was approximately 35 μm.

and above is accompanied by a violent ejection of liquid droplets from the sample. Figure 5 shows the time-sequenced images for $1.9\times10^{10}$ W/cm$^2$ which is slightly below the threshold irradiance. The early time images show the shock wave propagating into the ambient air. The shock wave is formed during the laser pulse by the pressure difference between the dense plasma and the ambient.[2,11] After the shock wave, images taken with delay up to 30 μsec reveal no measurable mass ejection from the surface.

Figure 6 shows the time-resolved images for ablation at $3.9\times10^{10}$ W/cm$^2$. As in Fig. 5, shock-wave propagation is observed shortly after the laser pulse. After the shock wave passes, there is a time period lasting 300-400 nsec where no mass removal is observed. At approximately 400 nsec after the laser pulse, mass leaving the silicon surface begins to appear. After 1 μsec delay, the images clearly show the ejection of molten or solid particulates. The ejection of these particulates lasted for about 30 μsec. A precise determination of the ejected particulate size is difficult due to the presence of diffraction rings around the particles in the images. Larger particles will have fewer diffraction rings and a sharper boundary; the size of the large particles in the image is estimated to be approximately 10 μm. Shadowgraph images for higher laser irradiance showed that more mass is ejected from

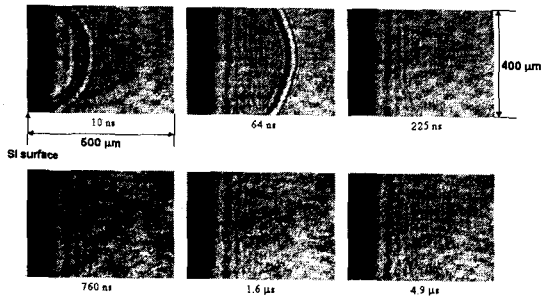


Fig.5 Sequence of shadowgraph images at laser irradiance of $1.9\times10^{10}$ W/cm$^2$; no measurable mass ejection is observed for this energy.

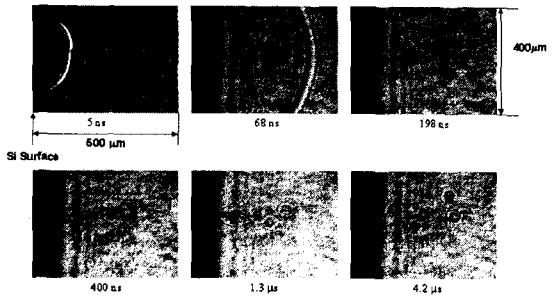


Fig.6 Sequence of shadowgraph images at laser irradiance of $3.9\times10^{10}$ W/cm$^2$; the ejection of particulates from the sample is clearly observed for this energy.

the sample with particulates as large as approximately 25-30 μm.

### 3.2 Analysis

A possible mechanism to describe the experimentally observed particulate ejection and deep-crater formation at a threshold is explosive boiling. Explosive boiling as a primary mechanism for mass removal during high power laser ablation was discussed in references 9 and 10. Normal boiling occurs under equilibrium conditions by heterogeneous nucleation at the solid-liquid interface or from microscopic gas inclusions. On the contrary, an explosive boiling occurs when the sample is heated rapidly and the molten layer becomes superheated; near the critical state. It is postulated that superheated liquid near the critical state experiences large density fluctuations,[12-14] which can generate vapor bubbles in the superheated volume. Once these vapor bubbles grow to a size greater than a critical radius, $r_c$, they expand spontaneously; bubbles less than $r_c$ are likely to collapse.[14] If vapor bubbles of size $r_c$ are generated in the entire superheated volume, the superheated liquid undergoes a rapid transition into a mixture of vapor and liquid droplets whose expansion leads to the violent ejection of mass, an explosive boiling.

For an explosive boiling to occur in the superheated liquid silicon, it is required that the vapor nuclei grow to the critical size. The time for vapor nuclei to grow to $r_c$ in the superheated liquid silicon near the critical state, $\tau_c$, is considered to be closely related to the time delay of mass ejection observed in the shadowgraph images. This time is determined below. Also, the thickness of the superheated liquid layer was estimated and compared with the deep-crater depths. In the case of explosive boiling, the crater depth may be represented by the superheated liquid thickness near the critical state at the time the bubbles reach $r_c$.

The critical radius and the time for a spherically symmetric bubble in a superheated liquid volume to grow to the critical radius can be expressed as [14]

$$r_c = \frac{2\sigma}{P_{sat}(T_l)\exp\{\upsilon_l[P_l - P_{sat}(T_l)]/RT_l\} - P_l} \qquad (1.a)$$

$$\tau_c = \left\{\frac{2}{3}\left[\frac{T_l - T_{sat}(P_l)}{T_{sat}(P_l)}\right]\frac{H_{l\upsilon}\rho_\upsilon}{\rho_l}\right\}^{-1/2} \qquad (1.b)$$

where $\sigma$ is the surface-tension coefficient, $P_l$, $\upsilon_l$, and $T_l$ are the pressure, specific volume, and temperature of the superheated liquid, respectively, $P_{sat}$ is the saturation pressure at the superheated liquid temperature, $R$ is the gas constant, $\rho$ is density, and $H_{l\upsilon}$ is the latent heat of vaporization. Because the critical temperature of silicon is unknown, it was assumed to be 5000 K, which is an average value for common metals such as aluminum, zinc, copper, silver, etc.[15] Large density fluctuations in a superheated liquid are reported to occur at 0.8-0.85 $T_c$, where $T_c$ is the ctritical temperature.[9,10] To compute $r_c$, $T_l$ was assumed to lie in this temperature range, namely $0.83T_c$. $P_{sat}(T_l)$ was obtained from the Clausius-Clayperon relation. The recoil pressure of the evaporating vapor, $0.54P_{sat}(T_l)$,[2] was approximated to be the pressure of the superheated liquid silicon layer, $P_l$. Aside from an arbitrary assumption of the critical temperature to be 5000 K, lack of knowledge on the variation of surface tension near the critical state for liquid silicon could result in a substantial uncertainty in the estimated $r_c$ and the bubble growth time. Therefore, the calculation is only expected to yield an order of magnitude for the estimated values. The surface tension of liquid silicon at the melting temperature is 0.73 N/m.[16] Surface tension coefficient drops as the temperature of the liquid increases. Yoshida[17] suggested a power law relation for $\sigma$ for liquid metals near the critical state. If the same relation applies to liquid silicon, a reduction of nearly 80% would occur in the value of $\sigma$ at the assumed $T_l$. Thus, the range of $\sigma$ during laser heating would be from 0.14 to 0.73 N/m, which yields $r_c$ ranging from 0.8 to 4.0 μm by Eq. (1.a). With this estimated $r_c$, $\tau_c$ is determined to be 90-490 nsec. The estimated bubble growth time is consistent with the measured time delay for particulate ejection (300-400 nsec). This agreement between the experimental delay time and calculated bubble growth time suggests that mass ejection delay time may be associated with the time for vapor bubbles to grow to the critical size in the superheated liquid and for explosive boiling to occur.

Depth of the superheated liquid layer near the critical state during and after the laser pulse was estimated with a numerical model. To solve the time-dependent temperature profile in the sample, the following conservation of energy equation for laser heating of solids was used:

$$\rho C\frac{\partial T}{\partial t}-\rho C v\frac{\partial T}{\partial x}=\frac{\partial}{\partial x}\left(k\frac{\partial T}{\partial x}\right)+I_0(t)\alpha\exp(-\alpha x) \quad (2)$$

where $\rho$ is density of the sample, $C$ is specific heat, $v$ is the receding velocity of the sample surface during evaporation, $k$ is thermal conductivity, $I_0$ is the temporal laser irradiance at the sample surface, and $\alpha$ is the absorption coefficient of the sample material at the incident laser wavelength. The spatial coordinate $x$ is in the direction normal to the sample surface with the origin located at the surface. An enthalpy formulation was employed to carry out the computation. The details of enthalpy formulation are discussed in Refs. 18-20.

The velocity $v$ in Eq. (2) is the receding velocity of the sample surface during evaporation and is represented by

$$v=\frac{\dot{m}_v}{\rho_l} \quad (3)$$

where $\dot{m}_v$ is the mass flux of vapor evaporated from the liquid surface and calculated using the Hertz-Knudsen formula[21,22]

$$\dot{m}_v(T_0)=p_{sat}(T_0)\left(\frac{m_a}{2\pi k_B T_0}\right)^{-1/2} \quad (4)$$

where $m_a$ is the atomic mass of silicon and $k_B$ is Boltzmann constant. Subscript 0 represents the evaporation surface. It was assumed that there is no significant recondensation of evaporated molecules. The boundary condition at the sample surface, i.e. at $x$=0, was set to be adiabatic when there is no surface evaporation. When vaporization exists at the surface, the energy loss was calculated as the latent heat of the evaporating mass.

When a metallic sample is heated close to the critical temperature, for example, by intense laser irradiation, the liquid metal becomes almost transparent to the incident laser radiation, by transforming into a liquid dielectric.[23-25] This phenomenon is called induced-transparency or bleaching of liquid metals, and is known to occur at a temperature of about $0.9T_c$. When the temperature of a thin liquid layer close to the sample surface is risen to $0.9T_c$, this liquid layer becomes transparent and the incident laser energy penetrates through this transparent layer to the underlying material. Because the liquid below the transparent layer may also reach $0.9T_c$ by subsequent heating, the transparent front propagates into the interior liquid until laser heating ceases. The optical properties of liquid silicon are reported to be similar to those of liquid metals.[26,27] It is therefore modeled that when liquid silicon is heated to $0.9T_c$, it may become transparent to the incident laser radiation. Note that the rate of evaporation at $x$=0 during the induced-transparency period remains constant at the value given by the Hertz-Knudsen relation, Eq.(4), at $0.9T_c$. The energy to maintain this evaporation rate is provided from the incident laser radiation.

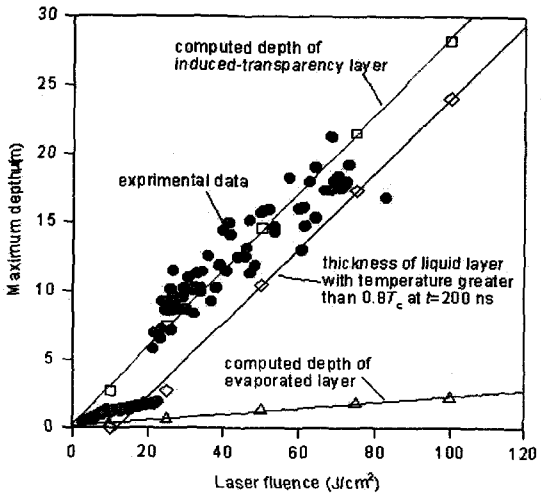


Fig.7 Comparison of measured crater depth (●) with computed data (□: maximum depth of induced-transparency layer; ◇: thickness of liquid layer with temperature over $0.8T_c$ at $t$=200 nsec; △: evaporation depth)

When the laser pulse is ceased, the propagation of induced-transparency front into the liquid silicon stops immediately, rendering the thickness of the induced-transparency layer to start shrinking. The temperature at $x$=0 also drops below $0.9T_c$ and thus the receding velocity $v$ in Eq.(3) becomes smaller than that at $0.9T_c$; however, the evaporation continues until the surface temperature decreases below the normal boiling temperature. For $t > \tau_p$, where $\tau_p$ is the laser pulse duration, the energy for evaporation is supplied from the interior liquid and as a result the temperature profile in the liquid has a maximum below the sample surface.

Gaussian energy distribution was chosen as the laser pulse source. The total pulse duration and pulse width at $1/e$ of the maximum intensity were 6 and 3 nsec, respectively, with the maximum located at 3 ns. Laser fluences, $F$, from 10 to 100 J/cm$^2$ were used in the calculations. The spatial domain of 50 or 100 μm (depending upon the laser fluence) was uniformly divided with a grid size of 12.5 nm; results obtained for smaller grid sizes differed by a negligible amount. Time steps of 1 ps were used. The thermal and optical properties of silicon used in the computation were found in Refs. 26-28. The initial temperature of the sample was 300 K.

Figure 7 summarizes the results for a numerical computation at selected laser fluences. In this figure, the measured crater depths in Fig. 2 were plotted with respect to laser fluences adjusted for plasma shielding, accounting for energy losses in the plume. According to Mao and Russo[29], the transmitted energy decreased to

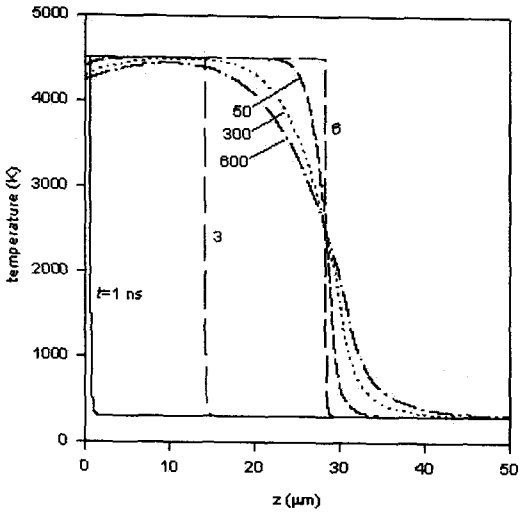


Fig.8 Temperature distribution inside the sample at different elapsed times (induced-transparency model, $F$=100 J/cm$^2$)

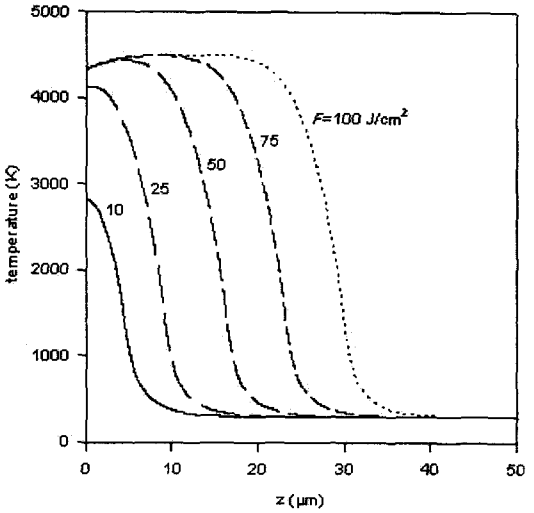


Fig. 9 Temperature distribution inside the sample for different laser fluences after 200 nsec from the laser pulse (induced-transparency model, $F$=100 J/cm$^2$)

about 20% of the original pulse energy due to plasma shielding as the laser power density increased to about 60 GW/cm$^2$. The thickness of the evaporated layer in Fig. 7 was computed by integrating the receding velocity of the surface without assuming the condition of induced transparency. The data show that, if evaporation were considered alone as a mechanism for mass removal above the threshold fluence, the computed depth underestimates the measured depth by an order of magnitude. Therefore, thermal evaporation alone is not adequate to account for the measured crater depth data.

The maximum thickness of the induced-transparency layer in Fig. 7 was computed with assuming the critical temperature of silicon to be 5000 K. To check the influence of the selected critical temperature on the calculated results, the thickness of the transparent layer for different values of $T_c$ was computed. The thickness of the transparent layer decreased by about 40% as the critical temperature was varied from 5000 to 9000 K, demonstrating that the order of magnitude of the computed transparent layer thickness is not significantly affected by the selected critical temperature. The computed thickness of the transparency layer in Fig. 7 is consistent with the measured crater depths for laser fluences above the threshold value, about 25 J/cm$^2$. More importantly, the agreement in the slopes of the measured crater depth and the computed transparency-layer thickness demonstrates that induced-transparency of the liquid silicon during laser ablation is a possible process in this energy regime. Because of the uncertainties in the present calculations, e.g., the thermodynamic critical temperature and optical properties of silicon at high temperatures, the value of the computed transparency layer thickness can be shifted either to higher or lower values.

The computed thickness of the induced-transparency layer itself does not represent the measured crater depth. Instead, the transparency layer provides the conditions that may lead to the generation of deep craters, that is, explosive boiling (phase explosion). For phase explosion to take place, the molten silicon should maintain the superheated state for time duration long enough for bubbles to grow to the critical size; an approximate estimation above showed that this time duration for superheated liquid silicon can range from 90 to 490 nsec. The computed temperature distribution inside the sample at different times shows that after 600 nsec from the beginning of laser irradiation, the thickness of the liquid layer that is at temperatures above $0.8T_c$ is more than 20 μm for $F$=100 J/cm$^2$ (cf. Fig. 8). Therefore, the liquid within 20 μm of the surface has sufficient time to allow vapor bubbles to grow to the critical size.

The thickness of the liquid layer that has temperatures above $0.8T_c$ after a necessary delay time varies with laser pulse energy. For $F$=10 J/cm$^2$, the thickness of the induced-transparency layer is about 2.7 μm. However, after 200 nsec, this transparency layer disappears completely (cf. Fig. 9), implying that the vapor bubbles would not have enough time to grow to the critical size and that no phase explosion would occur. For $F$=25 J/cm$^2$, the thickness of the induced-transparency layer is about 12 μm. For this laser fluence, at $t$=200 nsec, the thickness of the liquid layer that has temperatures above $0.8T_c$ is about 3.0 μm and a phase explosion can occur in this region. The thickness of the liquid layer with temperatures above $0.8T_c$ at $t$=200 nsec increases linearly with the same slope as the induced-transparency layer thickness and the measured crater depths (cf. Fig. 7). These results demonstrate that for laser ablation with fluences of 25 J/cm$^2$ or greater, the induced-transparency layer is sufficiently thick to permit

phase explosion of the superheated liquid.

## 4. CONCLUSION

Mass removed by high irradiance ($10^9$-$10^{11}$ W/cm$^2$) laser ablation on pure silicon was investigated by measuring the crater morphology with a white light interferometric microscope and imaging the mass ejection from the sample surface using shadowgraphy. The crater morphology shows a dramatic increase in crater depth at $2.2\times10^{10}$ W/cm$^2$. Above this threshold fluence, crater depths as large as 20 μm were produced from a single laser pulse, and they were deeper approximately by an order of magnitude from the depths below the threshold value. Thermal evaporation significantly underestimates the measured depth, especially for the fluence regime above the threshold value. For fluences above the threshold value, a good agreement is obtained between the measured crater depth and the calculated superheated liquid layer that satisfies explosive boiling conditions. These results support that induced transparency and explosive boiling may play an important role in forming the deep craters. Induced transparency promotes formation of the deep superheated liquid layer, which is thick enough to remain near the critical state long after the laser pulse. Vapor bubbles generated in this superheated liquid layer will have sufficient time to grow to the critical size, and a subsequent spontaneous expansion of them initiates an explosive boiling and mass ejection in the form of particulates.

## NOTICE

This research work has been published lately in Refs. 30 and 31.

## REFRENCES


(1) W. W. Duley, 1996, *UV Lasers: Effects and Applications in Materials Science*, Cambridge University Press, Cambridge, UK

(2) M. Von Allmen, 1987, *Laser Beam Interactions with Materials*, Springer, Heidelberg

(3) M. A. Shannon, X. Mao, A. Fernandez, W. T. Chan, and R. E. Russo, 1995, Analytical Chemistry, Vol. 67, p.4522

(4) A. Fernandez, X. L. Mao, W. T. Chan, M. A. Shannon, and R. E. Russo, 1995, Analytical Chemistry, Vol. 67, p. 2444

(5) S. H. Jeong, O. V. Borisov, J. H. Yoo, X. L. Mao, and R. E. Russo, 1999, Analytical Chemistry, Vol. 71, p.5123

(6) J. C. Miller and R. F. Haglund, Jr., 1991, *Laser Ablation Mechanisms and Ap-plications*, Springer, Heidelberg

(7) X. Zhang, S. S. Chu, J. R. Ho, and C. P. Grigoropoulos, 1997, Applied Physics A: Material Science and Processing, Vol. 64, p.545

(8) A. B. Brailovsky, S. V. Gaponov, and V. I. Luchin, 1995, Applied Physics A: Material Science and Processing, Vol. 61, p.81

(9) A. Miotello and R. Kelly, 1995, Applied Physics Letter, Vol. 67, p.3535

(10) R. Kelly and A. Miotello, 1996, Applied Surface Science, Vol. 96-98, p.205

(11) S. H. Jeong, R. Greif, and R. E. Russo, 1999, Journal of Physics D: Applied Physics, Vol. 32, p.2578

(12) M. M. Martynyuk, 1976, Soviet Physics Technical Physics, Vol. 21, 430

(13) M. M. Martynyuk, 1974, Soviet Physics Technical Physics, Vol. 19, 793

(14) V. P. Carey, 1992, *Liquid-Vapor Phase-Change Phenomena* Hemisphere, Washington

(15) M. M. Martynyuk, 1983, Russian Journal of Physical Chemistry, Vol. 57 p.494

(16) D. R. Lide, 1994, *CRC Handbook of Chemistry and Physics*, 75th ed. CRC, Boca Raton

(17) A. Yoshida, 1994, Journal of the Japan Institute of Metals, Vol. 58, p.1161

(18) J. R. Ho, C. P. Grigoropoulos, and J. A. C. Humphrey, 1995, Journal of Applied Physics, Vol. 78, p.4696

(19) N. Shamsundar and E. M. Sparrow, 1975, Journal of Heat Transfer, Vol. 97. p.333

(20) A. J. Dalhuijsen and A. Segal, 1986, International Journal for Numerical Methods in Engineering, Vol. 23, p.1807

(21) S. H. Jeong, R. Greif, and R. E. Russo, 1997, Proceedings of the ASME Heat Transfer Division, Vol. 351, p.68

(22) S. I. Anisimov, 1968, Soviet Physics JETP, Vol. 27, p.182

(23) V. A. Batanov, F. V. Bunkin, A. M. Prokhorov, and V. B. Fedorov, 1973, Soviet Physics JETP, Vol. 36, p.311

(24) R. V. Karapetyan and A. A. Samokhin, 1975, Soviet Journal of Quantum Electronics, Vol. 4, p.1141

(25) F. V. Bunkin and M. I. Tribelskii, 1980, Soviet Physics Uspekhi, Vol. 23, p.105

(26) R. O. Bell, M. Toulemonde, and P. Siffert, 1979, Applied Physics, Vol. 19, p.313

(27) I. Lukes, R. Sasik, and R. Cerny, 1992, Applied Physics A, Solids and Surfaces, Vol. 54, p.327

(28) O. Muller, S. De Unamuno, B. Prevot, and P. Dhamelincourt, 1996, Physica Status Solidi.A A, Applied Research, Vol. 158, p.385

(29) X. Mao and R. Russo, 1997, Applied Physics.A. Materials Science and Processing, Vol. 64, p.1

(30) J. H. Yoo, S. H. Jeong, X. L. Mao, R. Greif, and R. E. Russo, 2000, Applied Physics Letters, Vol. 76, p.783

(31) J. H. Yoo, S. H. Jeong, R. Greif, and R. E. Russo, 2000, Journal of Applied Physics, Vol. 88, p.1638